Available online at www.sciencedirect.com
ScienceDirect
International Journal of Solids and Structures 44 (2007) 3359–3378
INTERNATIONAL JOURNAL OF SOLIDS and STRUCTURES
www.elsevier.com/locate/ijsolstr

Delamination fracture analysis in the G_{II}–G_{III} plane using prestressed transparent composite beams

András Szekrényes *

Department of Applied Mechanics, Budapest University of Technology and Economics, H-1521 Budapest, P.O. Box 11, Hungary

Received 15 June 2006; received in revised form 10 September 2006
Available online 30 September 2006

Abstract

In this paper, the mixed-mode II/III version of the prestressed end-notched flexure fracture specimen is developed, which combines the well-known end-notched flexure and the modified split-cantilever beam specimens using a special rig. The new beam-like specimen is able to provide any combination of the mode-II and mode-III strain energy release rates. The mode-III part of the strain energy release rate is fixed by using the special rig, which loads the specimen in the plane of the delamination. The mode-II part of the strain energy release rate is provided by the external load using a three-point bending fixture. A simple closed-form solution using beam theory is developed for the strain energy release rates of the new configuration. The applicability and the limitations of the novel fracture mechanical test are demonstrated using unidirectional E-glass/polyester composite specimens. If only crack propagation onset is involved then the mixed-mode II/III prestressed end-notched flexure specimen can be used to obtain the fracture criterion of transparent composite materials in a relatively simple way.

Keywords: Variable mode-mixity; Beam theory; Three-point bending; Interlaminar fracture; Modified split-cantilever beam; End-notched flexure

1. Introduction

The interlaminar fracture is one of the most important subjects of the composite fracture mechanics. In the last three decades the attention of researchers and scientists was focused mainly on the mode-I, mode-II and mixed-mode I/II fracture characterization of composites. However, during the last years it has been recognized that the mode-III delamination is also essential for the complete fracture characterization of advanced composite materials. Not only the pure mode-III fracture but also the combined mode I/III and mode II/III cases should be elaborated.

For the investigation of the mode-I, mode-II and mixed-mode I/II interlaminar facture well-understood and standardized tools are available for the engineers and designers disposal. The double-cantilever beam

* Tel.: +36 1 463 1170; fax: +36 1 463 3471.
E-mail address: szeki@mm.bme.hu

0020-7683/$ - see front matter © 2006 Elsevier Ltd. All rights reserved.
doi:10.1016/j.ijsolstr.2006.09.029

(DCB, mode-I) (e.g., Williams, 1989;Olsson, 1992) the end-notched flexure (ENF, mode-II) (e.g., Carlsson et al., 1986; Schön et al., 2000) and the mixed-mode-bending (MMB, mixed-mode I/II) (Crews and Reeder, 1988; Reeder and Crews, 1990) specimens are the most popular tools in this respect. However, considering the latter two modes the possibilities are large. The end-loaded split (ELS) specimen (Davies et al., 1996; Wang and Vu-Khanh, 1996), the stabilized end-notched flexure (SENF) (e.g., Davies et al., 1996), the four-point bend end-notched flexure (4ENF) (Schuecker and Davidson, 2000) the tapered end-notched flexure (TENF) (Edde and Verreman, 1995; Qiao et al., 2003b) and the over-notched flexure (ONF) (Wang et al., 2003; Szekrényes and Uj, 2005) coupons should be mentioned as possible alternatives in mode-II fracture.

There is also a large number of tools for mixed-mode I/II fracture investigation; see, e.g., the work by Davidson and Sundararaman (1996). Only those are mentioned here, which satisfies the most important criterion against a mixed-mode I/II tool, namely the ability of varying the ratio of the mode-I and mode-II strain energy release rates (SERR) in a wide range. The asymmetric DCB (ADCB) specimen uses a complex loading fixture in order to load the two arms of the specimen with different forces (Bradley and Cohen, 1985). The variable mixed-mode (VMM) test (Hashemi et al., 1987) was also abandoned later, due to certain complications (e.g., the mode ratio changes with the crack length). In this respect the mixed-mode bending (MMB) specimen (Crews and Reeder, 1988; Reeder and Crews, 1990) is the most universal tool; although the complex fixture and the lack of a reliable experimental reduction technique make it difficult to apply in some cases. Ifju et al. (2002) and Chen et al. (2003) developed three new mixed-mode I/II configuration for stitched composites. The main advantage of these configurations is that the micro buckling of the fibers may be eliminated, although the test requires bonded steel tabs and a complex loading rig. The next step was made by Sørensen et al. (2004), so the DCB specimen loaded by uneven bending moments (DCB-UBM) was developed. This configuration promotes stable crack propagation at any mode ratio and enables the determination of the mixed-mode cohesive laws. The drawbacks of the test are that the complex fixture and the bonded steel tabs make it expensive to be manufactured. Furthermore, the data can be reduced only by an analytical solution. Finally, the prestressed end-notched flexure (PENF) specimen should be mentioned, which was developed by the present author (Szekrényes, 2006a). Although the PENF has several disadvantages (mode ratio changes with the crack length, the mode ratio can be calculated only after the experiment has been performed, only crack initiation measurements can be investigated) the test uses only a three-point bending setup and steel rollers to fix the crack opening. So it seems to be the most inexpensive system.

For the mode-III fracture there are also several possibilities. The crack-rail shear (CRS) system (Becht and Gillespie, 1988) and the split-cantilever beam (SCB) (Donaldson, 1988; Hwang and Hu, 2001; Naik et al., 2002) are ones of the earliest developments. The drawback of these tests is the significant mode-II contribution to the total SERR and that due to the low compliance values the compliance calibration (CC) method can not be applied. The SCB configuration was significantly modified by Sharif et al. (1995) and Trakas et al. (1997), so the modified split-cantilever beam (MSCB) was developed. The specimen was loaded by special grips and the mode-II SERR component was substantially reduced. The most important feature of the MSCB specimen is that it maintains the traditional beam-like geometry. The edge-crack torsion (ECT) specimen is considered as a significant contribution to the mode-III fracture developments (Lee, 1993; Liao and Sun, 1996; Suemasu, 1999). The ECT specimen produces about a 92% mode-III test and the compliance calibration technique can be applied for data reduction. Other possibilities for mode-III testing are the anti-clastic plate bending (ACPB) (Farshad and Flüeler, 1998; Podczeck, 2001), the splitting specimen discussed by Ehart et al. (1998, 1999) and the mode-III version of the 4ENF specimen (Yoshihara, 2006), which produces a 90% mode-III contribution to the total SERR along the crack front. Unfortunately, these configurations involve difficult coupon geometry and do not seem to be optimal solutions for composites.

There are also a lot of work dealing with the combination of the mode-I, mode-II and mode-III fracture modes. However, these works are related mainly for the testing of metals (Lazarus et al., 2001; Kamat et al., 1998; Li et al., 1995) and adhesive joints (e.g., Fernlund et al., 1995). The former works proposes the modified compact tension (CT) or the single edge notched bending (SENB) specimen with a skew made crack. In this manner a closed-form solution can not be developed (only a numerical one). Despite the really huge literature in this area, it seems that a useful beam-like specimen is missing for the characterization of the mixed-mode II/III fracture of composite materials.

The main object of this paper is to develop a mixed-mode II/III tool for interlaminar fracture testing using a beam-like specimen with variable mode ratio. Referring to the mixed-mode I/II version of the PENF specimen (denoted as $PENF_{I/II}$) (Szekrényes, 2006a) the idea may be extended for the case of the mixed-mode II/III loading. From this point of view the only alternative is the combination of the ENF and the MSCB specimens. This tool is denoted here as the $PENF_{II/III}$ specimen. The concept of the $PENF_{II/III}$ specimen can be seen in Fig. 1. In previous works accurate beam models were developed for the ENF (Szekrényes, 2005) and MSCB (Szekrényes, submitted for publication) specimens. These solutions are applicable for the $PENF_{II/III}$ by applying the principle of superposition. The schematic illustration of the MSCB specimen is demonstrated in Fig. 2. According to Fig. 2 a special rig transfers a scissor load to the specimen arms leading to a 97.8% mode-III fracture in the optimal case, which can be reached by properly choosing the geometrical parameters of the system. The mixed-mode II/III condition can be obtained in the following way. The ENF specimen can be prestressed using the rig of the MSCB specimen by a prestressing screw with pitch of 1.75 mm (refer to Fig. 6), which can fix the mode-III SERR. Then the prestressed ENF specimen is put into a three-point bending setup and the applied load at the center of the specimen can be increased up to fracture initiation. The latter produces the mode-II part of the system. Although in the $PENF_{II/III}$ specimen the mode ratio changes with the crack length and the mode ratio can not be designed, the system can be used to obtain the fracture criterion for transparent composite materials in a relatively simple way.

2. The PENF specimen for mixed-mode II/III cracking

2.1. Strain energy release rate and mode ratio

The $PENF_{II/III}$ specimen is the combination of the ENF and MSCB specimens. Fig. 1 shows that the crack tearing displacement (CTD), and so the mode-III part of the SERR is fixed by using a prestressing rig, which transfers the load related to the mode III condition (P_{MSCB}). For the analysis of the new configuration, we apply the superposition of the ENF and MSCB specimens referring to some previous works (Szekrényes, 2005, submitted for publication). The compliance of the ENF specimen is:

$$C_{\mathrm{ENF}} = \frac{3a^3 + 2L^3}{8bh^3E_{11}} + \frac{2L}{8bhkG_{13}} + \frac{a^3}{8bh^3E_{11}} f_{\mathrm{SH1}}, \tag{1}$$

where a is the crack length, L is the half span length, b is the width, h is the half thickness, $k = 5/6$ is the shear correction factor, E_{11} is the flexural modulus and G_{13} is the shear modulus of the material in the x–z plane, furthermore, the first term is from bending, the second one is from transverse shear and the last term accounts for crack tip shear deformation (Wang and Qiao, 2004). Furthermore

$$f_{\mathrm{SH1}} = 0.98\left(\frac{h}{a}\right)\left(\frac{E_{11}}{G_{13}}\right)^{\frac{1}{2}} + 0.43\left(\frac{h}{a}\right)^2\left(\frac{E_{11}}{G_{13}}\right). \tag{2}$$

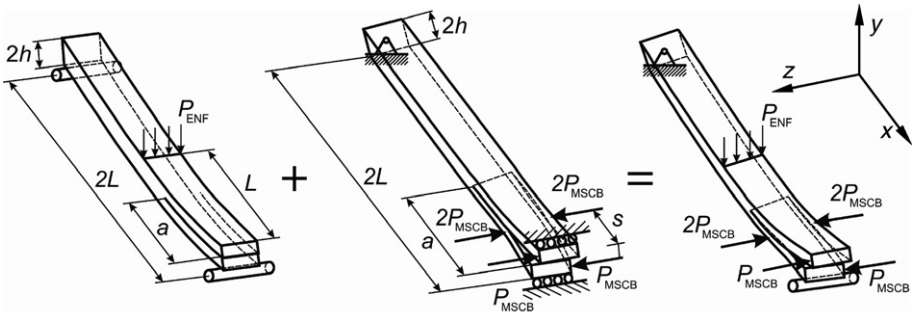

(a) ENF specimen mode-II (b) MSCB specimen mode-III (c) $PENF_{II/III}$ specimen mixed-mode II/III

Fig. 1. The mixed-mode II/III PENF specimen (c) as the superposition of the ENF (a) and MSCB (b).

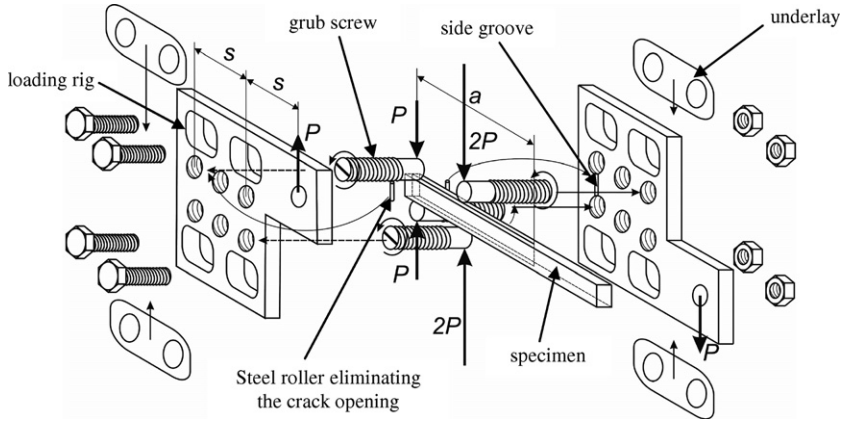

Fig. 2. Exploded view of the Modified Split-Cantilever Beam.

The SERR of the ENF specimen can be obtained by using the Irwin–Kies expression (Anderson, 2005)

$$G_C = \frac{P^2}{2b}\frac{\mathrm{d}C}{\mathrm{d}a}. \tag{3}$$

Thus we have

$$G_{\mathrm{II}} = \frac{P_{\mathrm{ENF}}^2 a^2}{16 b^2 h^3 E_{11}}[9 + f_{\mathrm{SH2}}], \tag{4}$$

where P_{ENF} is the load required for crack initiation, furthermore

$$f_{\mathrm{SH2}} = 1.96\left(\frac{h}{a}\right)\left(\frac{E_{11}}{G_{13}}\right)^{\frac{1}{2}} + 0.43\left(\frac{h}{a}\right)^2\left(\frac{E_{11}}{G_{13}}\right). \tag{5}$$

For the analysis of the MSCB specimen a recent work is referred to (Szekrényes, submitted for publication), in which an accurate beam model was developed taking four mechanical deformations into account: bending and shearing of the specimen arms, the Saint-Venant effect at the crack front and the free torsion effect in the delaminated area. The compliance and the SERR calculated by the analytical solution were compared to the results of a three-dimensional finite element model and an excellent agreement was found. The compliance of the MSCB specimen is

$$C_{\mathrm{MSCB}} = \frac{8a^3}{b^3 h E_{11}}[f_{\mathrm{EB1}} + f_{\mathrm{TIM1}} + f_{\mathrm{FT1}} + f_{S\text{-}V1}], \tag{6}$$

where the terms in the brackets consider bending, transverse shear, free torsion and Saint-Venant effect in the MSCB specimen

$$f_{\mathrm{EB1}} = 1 - 6\left(\frac{s}{a}\right) + 12\left(\frac{s}{a}\right)^2 - 6\left(\frac{s}{a}\right)^3, \tag{7}$$

$$f_{\mathrm{TIM1}} = 0.3\left(\frac{b}{a}\right)^2\left(\frac{E_{11}}{G_{13}}\right), \tag{8}$$

$$f_{\mathrm{FT1}} = 0.19\frac{1}{\varsigma}\left(\frac{b}{a}\right)^2\left(\frac{E_{11}}{G_{12}}\right), \tag{9}$$

$$f_{S\text{-}V1} = \left[0.48 - 1.91\left(\frac{s}{a}\right) + 1.91\left(\frac{s}{a}\right)^2\right]\left(\frac{b}{a}\right)\left(\frac{E_{11}}{G_{13}}\right)^{\frac{1}{2}}, \tag{10}$$

and

$$\varsigma = 1 - 0.63\mu\frac{h}{b}, \quad \mu = \left(\frac{G_{13}}{G_{12}}\right)^{\frac{1}{2}}, \tag{11}$$

where s is the distance between the loads of the specimen arms (refer to Fig. 1), G_{12} is the shear modulus of the material in the x–y plane. The SERR rate may be obtained by using Eq. (3), this results in

$$G_{\mathrm{III}}^{97.8\%} = \frac{12P_{\mathrm{MSCB}}^2 a^2}{b^4 h E_{11}}[f_{\mathrm{EB2}} + f_{\mathrm{TIM2}} + f_{\mathrm{FT2}} + f_{S\text{-}V2}], \tag{12}$$

where P_{MSCB} is the load required for crack initiation, furthermore

$$f_{\mathrm{EB2}} = 1 - 4\left(\frac{s}{a}\right) + 4\left(\frac{s}{a}\right)^2, \tag{13}$$

$$f_{\mathrm{TIM2}} = 0.1\left(\frac{b}{a}\right)^2\left(\frac{E_{11}}{G_{13}}\right), \tag{14}$$

$$f_{\mathrm{FT2}} = 0.06\frac{1}{\varsigma}\left(\frac{b}{a}\right)^2\left(\frac{E_{11}}{G_{12}}\right), \tag{15}$$

$$f_{S\text{-}V2} = \left[0.32 - 0.64\left(\frac{s}{a}\right)\right]\left(\frac{b}{a}\right)\left(\frac{E_{11}}{G_{13}}\right)^{\frac{1}{2}}. \tag{16}$$

In Eq. (12) the sign of 97.8% in the superscript refers to the optimal case, when the mode-II component of the SERR is substantially reduced. The optimal geometrical parameters of the MSCB were determined based on finite element calculations (Szekrényes, submitted for publication). In order to obtain a test, which produces a nearly 98% mode-III test the restriction is

$$2.00 \leqslant a/s \leqslant 2.23. \tag{17}$$

In the present study $s = 26$ mm was used, so the crack length of interest was chosen to be $a = 55$ mm, this gives $a/s = 2.115$, which satisfies Eq. (17) and the mode-III SERR is 97.8% of the total SERR calculated by integrating the SERR along the crack front in finite element models. Using the prestressing rig the displacement of the MSCB specimen can be controlled. For this reason we express the force which arises in the MSCB specimen by using Eq. (6) and we use also the definition of $C_{\mathrm{MSCB}} = \delta_{\mathrm{MSCB}}/P_{\mathrm{MSCB}}$

$$P_{\mathrm{MSCB}} = \frac{b^3 h E_{11}\delta_{\mathrm{MSCB}}}{8a^3}\frac{1}{(f_{\mathrm{EB1}} + f_{\mathrm{TIM1}} + f_{\mathrm{FT1}} + f_{S\text{-}V1})}. \tag{18}$$

Substituting Eq. (18) into Eq. (12) we obtain

$$G_{\mathrm{III}}^{97.8\%} = \frac{3}{16}\frac{b^2 h E_{11}\delta_{\mathrm{MSCB}}^2}{a^4}\frac{(f_{\mathrm{EB2}} + f_{\mathrm{TIM2}} + f_{\mathrm{FT2}} + f_{S\text{-}V2})}{(f_{\mathrm{EB1}} + f_{\mathrm{TIM1}} + f_{\mathrm{FT1}} + f_{S\text{-}V1})^2}. \tag{19}$$

Combining Eq. (19) with (4) the mode ratio becomes

$$\frac{G_{\mathrm{III}}^{97.8\%}}{G_{\mathrm{II}}} = \frac{3b^4 h^4 E_{11}^2}{a^6}\left(\frac{\delta_{\mathrm{MSCB}}}{P_{\mathrm{ENF}}}\right)^2\frac{(f_{\mathrm{EB2}} + f_{\mathrm{TIM2}} + f_{\mathrm{FT2}} + f_{S\text{-}V2})}{(f_{\mathrm{EB1}} + f_{\mathrm{TIM1}} + f_{\mathrm{FT1}} + f_{S\text{-}V1})^2}\frac{1}{(9 + f_{\mathrm{SH2}})}. \tag{20}$$

Eq. (20) shows that the mode ratio (or the mode-III SERR) can be controlled by varying the crack tearing displacement using the prestressing rig of the MSCB specimen. If we increase the CTD then it is expected that the applied load (P_{ENF}) required for crack initiation will decrease. If we wish perform a crack propagation test under a fixed CTD and the crack length approaches to infinity, furthermore the mode-III SERR will subsequently decay and the system will tend to a pure mode-II problem. As a consequence, the mode ratio ($G_{\mathrm{III}}/G_{\mathrm{II}}$) also depends on the crack length.

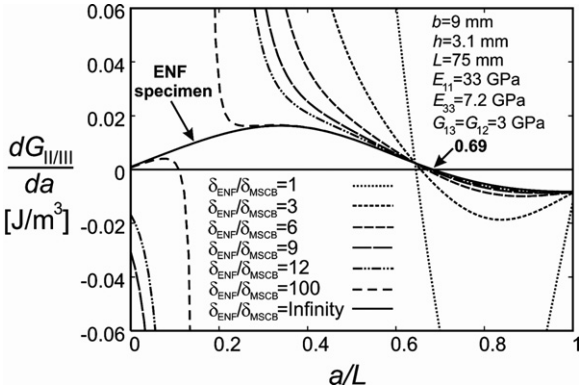

Fig. 3. Crack stability chart of the $PENF_{II/III}$ specimen.

2.2. Crack stability

The stability of the system is determined by the derivative of the strain energy release rate with respect to the crack length. If dG_C/da is zero or negative then stable crack propagation may be expected. We consider the case of fixed grip condition; in this case the derivative of the SERR is (Carlsson et al., 1986)

$$\frac{dG_C}{da} = \frac{\delta^2}{2bC^2}\left[\frac{d^2C}{da^2} - \frac{2}{C}\left(\frac{dC}{da}\right)^2\right]. \tag{21}$$

The solution can be obtained by combining Eq. (21) with Eqs. (4), (12) and (1), (6)

$$\frac{dG_{II/III}}{da} = \frac{dG_{II}}{da} + \frac{dG_{III}^{97.8\%}}{da}. \tag{22}$$

The solution of Eq. (22) for different cases is demonstrated in Fig. 3. The stability range of the PENF system does not change essentially, i e., the stability range is approximately the same as that of the ENF specimen

$$a \geqslant 0.69L. \tag{23}$$

3. Finite element analysis

The finite element analysis was performed in order to confirm the accuracy of the analytical solution. The $PENF_{II/III}$ specimen is the superposition of the ENF and MSCB specimens. For the ENF specimen the accuracy and applicability of Eq. (4) to data reduction has already been shown in the literature (Wang and Qiao, 2004; Szekrényes and Uj, 2006). To demonstrate the accuracy of the improved beam model (Eqs. (6) and (12)) of the MSCB specimen a simulated compliance calibration was performed.

For the calculation the COSMOS/M 2.0 package was used. The three-dimensional model of the MSCB specimen was built using linear eight-node SOLID brick elements. Similar models were used, for example, by Davidson et al. (1995), hence the model is not shown here. The elastic properties used the models are $E_{11} = 33$ GPa, $E_{22} = E_{33} = 7.2$ GPa, $G_{12} = G_{13} = G_{23} = 3$ GPa and $\nu_{12} = \nu_{13} = \nu_{23} = 0.27$. The geometrical properties are: $a = 55$ m, $b = 9$ mm, $2h = 6.2$ mm, $s = 26$ mm and the length of the models is $2L = 150$ mm (refer to Fig. 1). The models consisted of 18,624 elements, while the number of nodes – depending on the area of the crack faces – was about 23,000. The penetration of the nodes in the crack faces was eliminated by forcing them to have the same displacements in the y direction by using the command CPDOF. However, this command enables such restrictions only for 500 pairs of nodes. Since for greater crack lengths the number of node pairs was more than 500, only the nodes at the specimen sides were constrained. The elements of the model were checked and no errors or warnings were received. In each case, the mode-I SERR component was zero along the crack front.

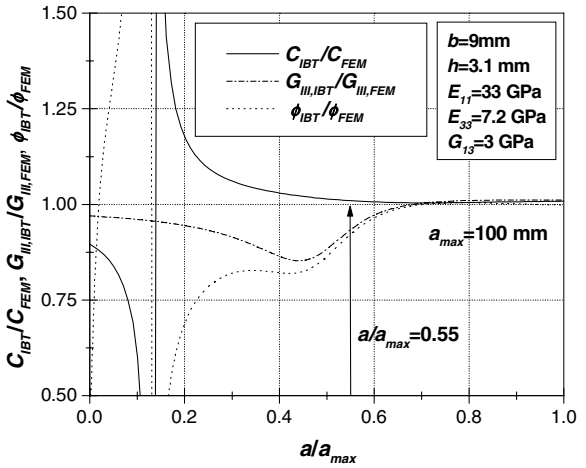

Fig. 4. Comparison of the compliance, the mode-III strain energy release rate of the MSCB specimen and the mode ratio of the $PENF_{II/III}$ specimen by beam and FE analysis.

For the MSCB specimen the boundary conditions of the finite element model are demonstrated in Fig. 1b. The model was loaded ($P = 1$ N) at four points (see Fig. 1b). The compliance of the MSCB specimen was determined in the crack length range of $a = 45\ldots105$ mm and was fitted by a full third order polynomial as a function of the crack length. Then the mode-III energy release rate was calculated by using Eq. (3). The mode ratio of the $PENF_{II/III}$ specimen was determined by using the former FE solution for the MSCB specimen and an accurate FE model by Bao et al. (1992) for the ENF specimen. Then the analytically determined mode ratio (ϕ_{IBT}, Eq. (20)) was divided by the numerically determined one (ϕ_{FEM}).

In Fig. 4 the ratio of the analytical and numerical compliances, SERRs of the MSCB specimen and the ratio of the analytical and numerical mode mix of the $PENF_{II/III}$ specimen are demonstrated against the normalized crack length. It is shown that at the ratio of $a/a_{max} = 0.55$ (which will be the case for the experiments) the compliance is very close to that predicted by the FE model, while the difference between the analytically and numerically determined SERRs is about 5–6% for the same a/a_{max} ratio. The mode mix of the $PENF_{II/III}$ system shows also about a 6% difference compared to the numerical results. Otherwise, the greater is the crack length the higher is the accuracy of the analytical solution.

4. The dependence of the mode ratio on the system parameters

Since the FE analysis showed the good accuracy of the analytical model it is reasonable to investigate the dependence of the mode ratio on certain parameters of the system. Figs. 5a and b show the variation of the mode ratio (Eq. (20)) against the normalized applied load and the crack length. The results in Figs. 5a and b were calculated by using the analytical solution (Eq. (20)) with the following geometrical and material properties: $b = 9$ mm, $h = 3.1$ mm, $L = 75$ mm, $s = 26$ mm, $E_{11} = 33$ GPa, $G_{13} = G_{12} = 3$ GPa and are strictly to demonstrate the changes in the mode ratio of the present E-glass/polyester material at given crack openings ($\delta_{MSCB} = 0.5$ and 2.0 mm in Fig. 5a, and $\delta_{MSCB} = 0.5$ and 3.0 mm in Fig. 5b). The maximal values of the applied load (P_{max}) and crack length (a_{max}) were chosen arbitrarily.

If the crack initiation takes place in the glass/polyester specimen investigated and we increase the load by 5 N it leads to about a +7.5% change in the mode ratio independently on the crack tearing displacement. The change of the crack length is more negligible: if crack initiation takes place and the crack length changes by 1 mm (and assuming that the load does not change) it will lead to a −2.5% change in the mode ratio. For a case, when the crack length of interest is $a = 55$ mm ($a/a_{max} = 0.733$), then the changes in the mode ratio by the applied load is very small. Thus the effect of applied load on the mode ratio is more significant, so the accurate identification of the crack initiation plays a very important role in the application of the $PENF_{II/III}$ specimen. On the one hand if the critical applied load is measured inaccurately, then the mode-II SERR (and so the mode ratio) will change. On the other hand it is essential that after crack initiation some increase in the crack length is expected, however it is

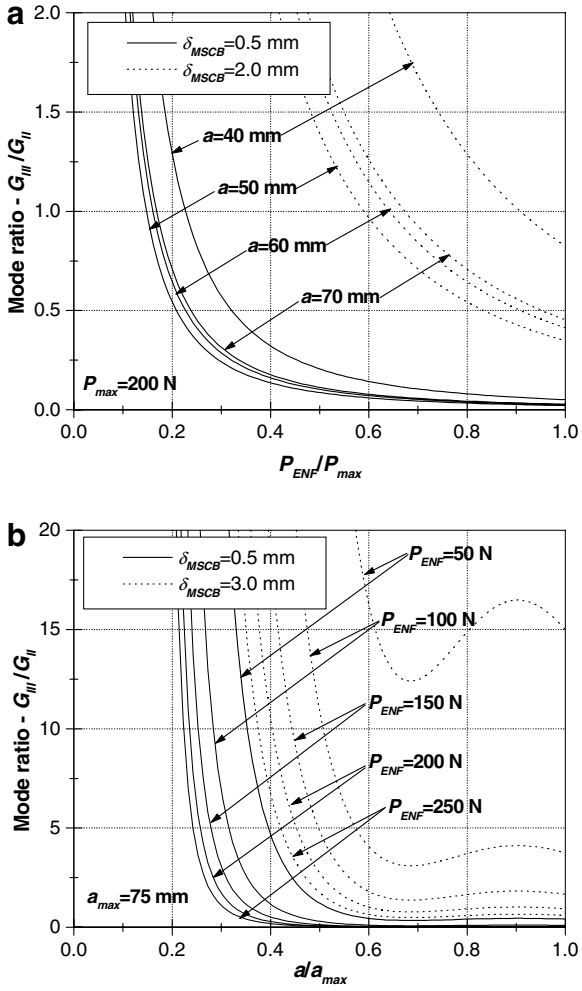

Fig. 5. Variation of the mode-ratio in the $PENF_{II/III}$ specimen as the function of the applied load (a) and the crack length (b).

assumed to be very small and this leads to only a little change in the mode ratio. Finally, after crack initiation the crack length increases, which decreases the mode ratio, it may be assumed that the applied load also increases and this decreases G_{III}/G_{II}. So, these two quantities have an opposite effect on the mode ratio.

If the material under consideration is non-transparent then the solution is for example the application of ultrasonic or acoustic emission equipment for the identification of the crack initiation.

Another feature of the $PENF_{II/III}$ system is that the mode ratio depends on the elastic properties of the material (refer to Eq. (20)). However, this fact does not influence the applicability of the system, because any mode ratio can be achieved independently of the type of the material.

In the following sections the performed experimental work is detailed, including mode-II, mode-III and mixed-mode II/III tests separately. Then the experimental data are reduced by using three methods: improved beam theory (IBT), compliance calibration (CC) and the finite element method (FEM). An optimal reduction technique is recommended for data evaluation. In the final section the fracture envelope in the G_{II}–G_{III} plane is demonstrated and compared to the one in the G_I–G_{II} plane for the same material.

5. Experiments

The constituent materials of the investigated E-glass/polyester composite were procured from Novia Ltd. The properties of the E-glass fiber are $E = 70$ GPa and $\nu = 0.27$, while for the unsaturated polyester resin are

$E = 3.5$ GPa and $v = 0.35$. Both were considered isotropic. The unidirectional ($[0°]_{14}$) E-glass/polyester specimens with nominal thickness of $2h = 6.2$ mm, width of $b = 9$ mm and fiber-volume fraction of $V_f = 43\%$ were manufactured in a special pressure tool. A polyamide (PA) insert with thickness of 0.03 mm was placed at the midplane of the specimens to make an artificial starting defect. A great advantage of the present E-glass/polyester material is the transparency, which allows of the visual observation of crack initiation/propagation. The tool was left at room temperature until the specimens became dry. Then the specimens were removed from the tool and were further left at room temperature until 4–6 h. The specimens were cut to the desired length and were precracked in opening mode of 4–5 mm by using a sharp blade. The reason for that was in this case it was possible to make a straight crack front, which is important in the case of the crack length measurement and the observation of the crack initiation. On the other hand, mode-II precracking can be achieved using, e.g., a three-point bending setup; however in this way the crack front would be non-uniform.

5.1. Material properties

The flexural modulus was determined from a three-point bending test with span length of $2L = 150$ mm using six uncracked specimens with $2h = 6.2$ mm and $b = 20$ mm. Then specimens were cut along the longitudinal direction in order to obtain very narrow specimens. The narrow specimens were rotated by 90° about the longitudinal axis compared to the original measurements and the modulus of the specimens was again measured. Both experiments resulted in $E_{11} = 33$ GPa, i.e., the material was found to be transversely isotropic. The additional properties were predicted from simple rules of mixture, in this way $E_{22} = E_{33} = 7.2$ GPa, $G_{12} = G_{13} = 3$ GPa and $v_{12} = v_{13} = 0.27$ were obtained. The material properties were used in the beam and finite element analyses.

5.2. End-notched flexure test

For the ENF test (Fig. 1b) four specimens with $a = 55$ mm and $2L = 150$ mm were prepared. The specimens were tested using an Amsler testing machine and were loaded until the point of fracture initiation. At this point the critical specimen displacement and the critical load were recorded. The displacement was measured using a mechanical dial gauge, while the values of the applied load were read from the scale of the testing machine.

5.3. Modified split-cantilever beam test

For the MSCB measurements four specimens were prepared with $a = 55$ mm and $s = 26$ mm. Each specimen was put into the loading rig shown in Fig. 2, the rig was adjusted in order to eliminate any play of the specimens. Then the specimens were loaded, the load and displacement values were read from the scale of the testing machine and using a mechanical dial gauge. Crack initiation was identified visually, so when the first non-uniformity concerning the straight crack front was observed it was believed to be the point of crack initiation.

5.4. Prestressed end-notched flexure test

The experimental equipment for the PENF test is demonstrated in Fig. 6. The tests were carried out using an Amsler testing machine under displacement control. The span length was $2L = 150$ mm, the crack length of interest was $a = 55$ mm. The reason for the latter was (apart from the optimal case discussed in Section 2) that the critical crack tearing displacement measured from the MSCB test is about 2.5 mm (if $a = 55$ mm) and the crack tip is far enough (20 mm) from the point of load application. The stiffness, the compliance and the mode-II SERR of the PENF specimen are identical to those of the ENF specimen. Six values of the displacement, δ_{MSCB} were set using the prestressing screw in order to control the mode-III part of the total SERR: $\delta_{\mathrm{MSCB}} = 0.875$, 1.313, 1.750, 2.023, 2.188 and 2.297 mm. These values were calculated by being aware of the pitch (1.75 mm) of the prestressing screw. It was assumed that the crack tearing displacements (δ_{MSCB}) in Eqs. (19) and (20) are equal to these values. As in the MSCB and ENF tests, we applied four coupons at each steel roller. The load-deflection data was measured by using the scale of the testing machine and the dial gauge (see Fig. 6).

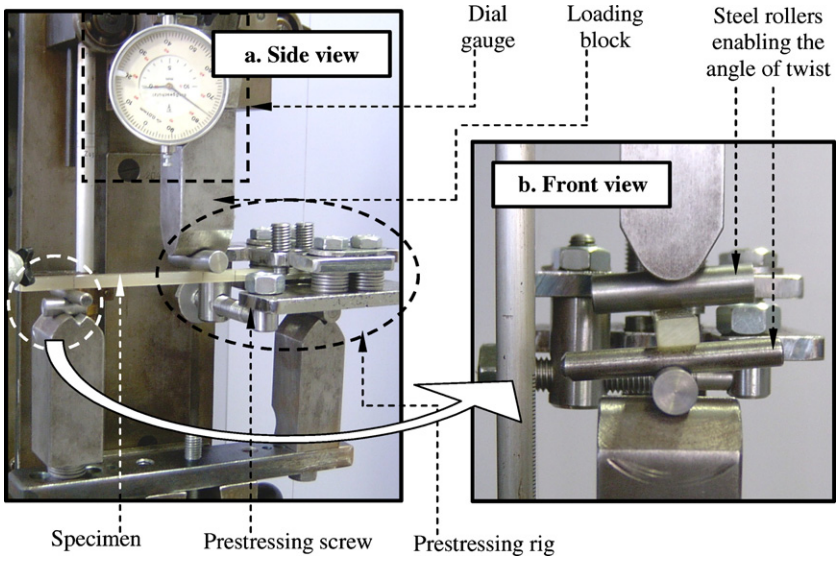

Fig. 6. The mixed-mode II/III prestressed end-notched flexure ($PENF_{II/III}$) specimen.

6. Results and discussion

6.1. Load and displacement

The recorded load-displacement curves are shown in Fig. 7 for the MSCB and ENF specimens. The responses follow approximately a linear relation, however, a very small nonlinearity was observed at the end of the curves. Crack onset was identified by visual observations. In each case four specimens were tested, one of them was used to investigate the crack front. The other three specimens were loaded continuously and the crack initiation was observed in situ. So, the former specimen was loaded subsequently, at some points, where the initiation was expected the specimen was relieved, removed form the bending setup and the crack front was photographed. When the first non-uniformity was observed, then this point was denoted as the point of fracture initiation. The results of this process are demonstrated in Fig. 8 for the $PENF_{II/III}$ system at a prestressed state with $\delta_{MSCB} = 1.75$ mm.

A comparison between Figs. 7b and 8a indicates that the fit curve of load-displacement traces of the ENF and $PENF_{II/III}$ specimens are eventually the same, so the prestressing rig does not influence the stiffness of the system and finally the compliance of the $PENF_{II/III}$ specimen is equal to that of the ENF one.

6.2. Data reduction

Three reduction techniques (IBT, CC and FEM) were applied to reduce the experimental data. The advantages and drawbacks of the different schemes are also discussed. It is also remarkable that for the mixed-mode I/II version of the PENF specimen four reduction schemes were applied: improved beam theory, simple beam theory (SBT), direct beam theory (DBT, see, e.g., Schön et al., 2000) and the compliance calibration. For mode-I and mode-II specimens the CC is thought to be the most accurate. In the relevant paper (Szekrényes, 2006a) the best agreement with the CC method was obtained by using the IBT method for the evaluation of G_I and the DBT for the calculation of G_{II}, i.e., a combined IBT–DBT scheme was recommended.

6.2.1. Improved beam theory

Modified split-cantilever beam. In Eq. (12) P_{MSCB} should be replaced with P_{III} (the load value for crack initiation in the MSCB specimen) in order to obtain the improved analytical expression for the SERR of the MSCB specimen.

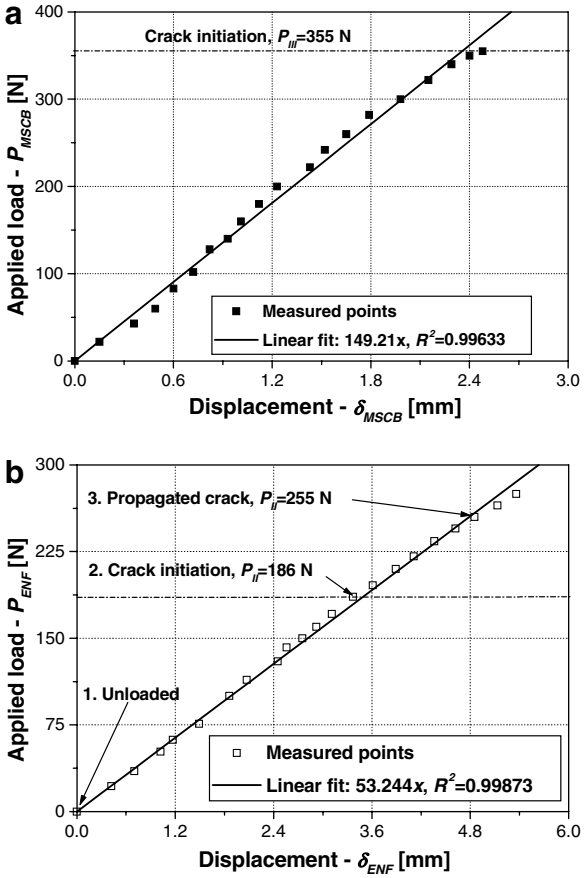

Fig. 7. Load-displacement curve of the MSCB (a) and ENF (b) specimens at $a = 55$ mm.

End-notched flexure specimen. Replacing P_{ENF} with P_{II} in Eq. (4) gives the improved solution for the ENF coupon, where P_{II} is the critical load value at crack onset.

Prestressed end-notched flexure specimen. The improved analytical solutions are given by Eqs. (4) and (19) for the $\mathrm{PENF_{II/III}}$ system.

It is remarkable that in general the additional material properties (G_{12}, G_{13}) of the material are not known with the desired accuracy. The reason for that is the different rules of mixture give only approximate results. Hence the results of the improved expressions should be used carefully.

6.2.2. Compliance calibration

End-notched flexure specimen. For the ENF test 10 specimens were used to determine the compliance curve of the system in the crack length range of $a = 25$–70 mm with 5 mm increments. Each specimen was loaded until fracture initiation. The compliance at each crack length was calculated and the values were fitted by a third order polynomial of the form (Schuecker and Davidson, 2000)

$$C_{\mathrm{ENF}} = C_{01} + ma^3, \tag{24}$$

where C_{01} and m were found by using least square fitting. In this case the mode-II SERR is

$$G^{\mathrm{CC}}_{\mathrm{II,ENF}} = \frac{P^2_{\mathrm{II}}}{2b}\frac{\mathrm{d}C_{\mathrm{ENF}}}{\mathrm{d}a}. \tag{25}$$

The SERR was determined for the same specimens that were used for obtaining the $C(a)$ curve (Eq. (24)).

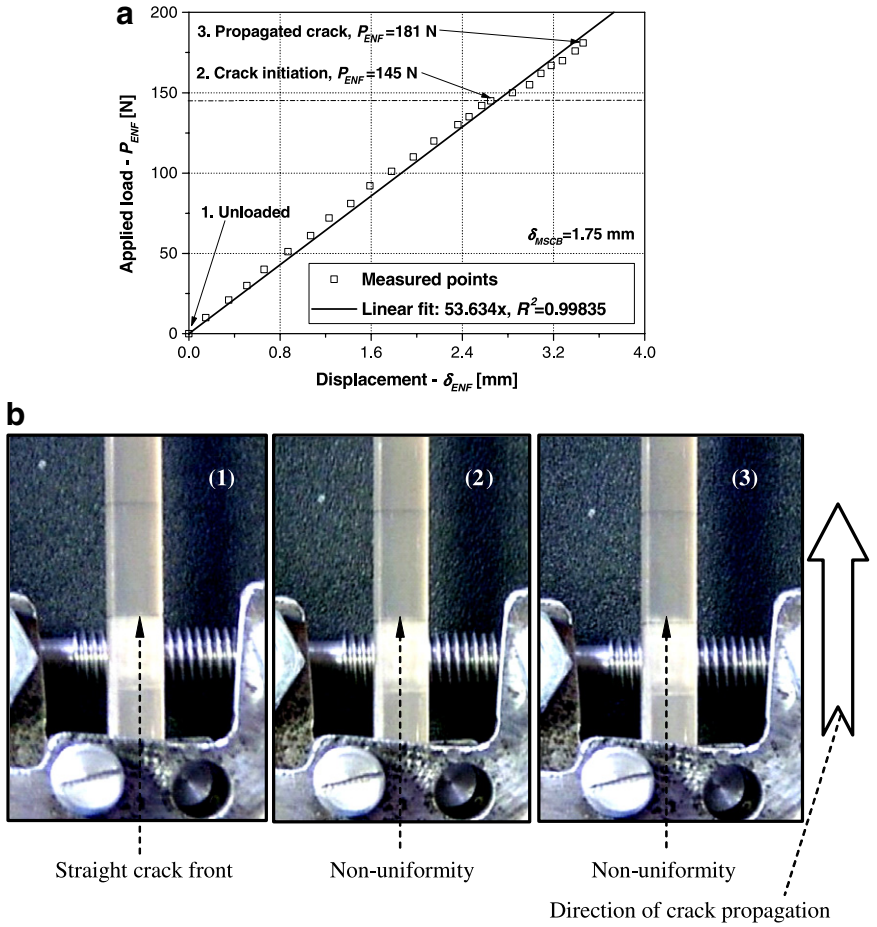

Fig. 8. Load-displacement curve of the $PENF_{II/III}$ specimen, $\delta_{MSCB} = 1.75$ mm (a). Non-uniformity of the crack front at the point of crack initiation (b).

Modified split-cantilever beam. For the MSCB test 12 specimens were prepared with crack lengths of $a = 45$, 50, 55, 60, 65, 70, 75, 80, 85, 90, 95 and 100 mm in order to determine the compliance of the MSCB system in a quite extended crack length range. Each specimen was loaded until fracture initiation. At each crack length the compliance of the specimens was determined, and then the compliance values were fitted with a third order polynomial of the form

$$C_{\mathrm{MSCB}} = C_0 + C_1 a + C_2 a^2 + C_3 a^3, \tag{26}$$

where the coefficients C_i, $i = 0\ldots3$ were determined by least square fitting, while the SERR was determined with the help of Eq. (3)

$$G^{\mathrm{CC}}_{\mathrm{III,MSCB}} = \frac{P^2_{\mathrm{III}}}{2b}\frac{\mathrm{d}C_{\mathrm{MSCB}}}{\mathrm{d}a}. \tag{27}$$

Prestressed end-notched flexure specimen. The mode-II and mode-III SERRs were determined by combining the results of the ENF and MSCB tests. The mode-II component by using the derivative of the ENF compliance curve (Eq. (24)) is

$$G^{\mathrm{CC}}_{\mathrm{II,PENF}} = \frac{P^2_{\mathrm{ENF}}}{2b}\frac{\mathrm{d}C_{\mathrm{ENF}}}{\mathrm{d}a}. \tag{28}$$

In order to calculate the force in the prestressing screw the slope of the load-displacement curve of the MSCB specimen at $a = 55$ mm was measured by using four coupons (refer to Fig. 7a). The results were averaged and were fitted with a linear function, which resulted in

$$P_{\mathrm{MSCB}} = 149.21 \cdot \delta_{\mathrm{MSCB}}. \tag{29}$$

Using the derivative of the MSCB compliance curve (Eq. (26)) the mode-III SERR is

$$G^{\mathrm{CC}}_{\mathrm{III,PENF}} = \frac{P^2_{\mathrm{MSCB}}}{2b}\frac{\mathrm{d}C_{\mathrm{MSCB}}}{\mathrm{d}a}, \tag{30}$$

where P_{MSCB} was obtained by the help of Eq. (29).

It is noteworthy that the application of the CC method is complicated in the case of the PENF specimen. The reason for that is it is not possible to test at a single mode ratio without performing ENF and MSCB tests. Furthermore, it is recommended to determine the compliances in a quite extended range of crack length, because the accuracy of the method depends on the number of points used for the curve-fit process. On the other hand specimen-to-specimen variation is not accounted for; this may cause problems if the specimens are fabricated using more than one composite plate. A significant advantage of this method is there is no need to determine the elastic properties of the material.

Fig. 9 shows the measured compliance values and the fitted curves of the ENF (Fig. 9a) and MSCB (Fig. 9b) data. Both curves fit the measured data well. For the sake of completeness even the analytical solutions (Eqs. (1) and (6)) are shown in Fig. 9a and b, indicating a very good agreement with the fitted curves.

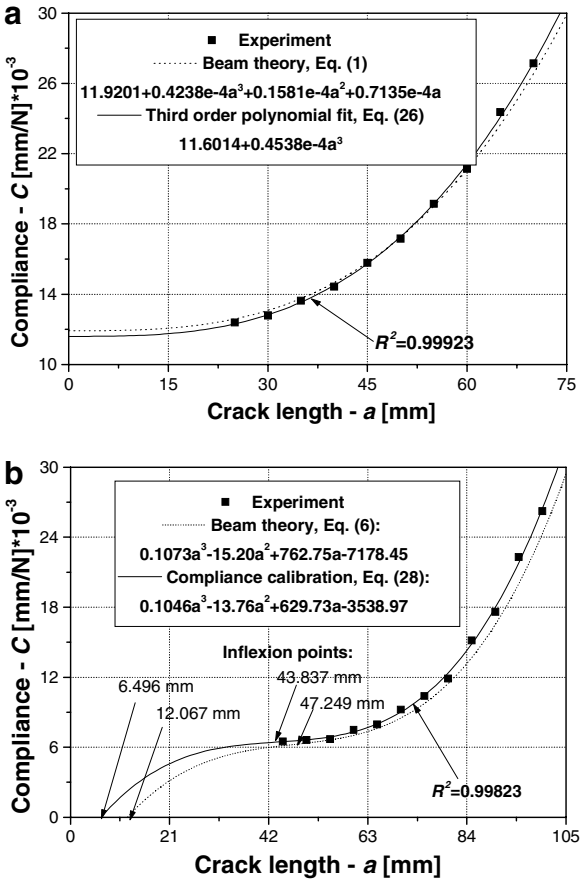

Fig. 9. The measured compliance values and the fit compliance curves of the ENF (a) and MSCB (b) specimens.

In the original work which presented the MSCB specimen (Cicci et al., 1995; Sharif et al., 1995) it was found that the CC method is inherently unreliable for data evaluation due to the following reasons: the specimen produces a very low compliance, the compliance is dominated by bending and finally the waviness of the delamination plane inducing friction between crack faces. In spite of these conclusions the good agreement between the theory and experiment in Fig. 9b can be explained by the followings:

- In the original papers (Cicci et al., 1995; Sharif et al., 1995) the authors manufactured the specimens from composite plates. This can lead to some inaccuracy, if the specimens are cut from different plates. In the present study, the specimens were manufactured in a special pressure tool. In this tool always the same number of fiber bundles and the same amount of polyester resin was used for a unique specimen. Even the size of the specimens was ensured to be the same.
- During the measurement of the MSCB specimen any play of the specimen should be eliminated, i.e., there should not be a space between the four grub screws and the specimen when the specimen is unloaded. This is important to eliminate the large scatter of the measured points.
- The original authors (Cicci et al., 1995; Sharif et al., 1995) reported that the compliance of the MSCB specimen is significantly lower than that of the usual mode-I and mode-II test. Comparing Fig. 9a to b we may conclude that for the same geometry: $C_{\mathrm{ENF}} = 12...28$ mm/N $^{*}10^{-3}$ $(a = 25...70$ mm) and $C_{\mathrm{MSCB}} = 6...28$ mm/N$^{*}10^{-3}$ $(a = 45...100$ mm). This indicates that the compliances have values in the same order, although in a different crack length range.

In spite of that it may be expected that for other types of composite material the problems of the CC method listed above take place, hence it does not seem to be the optimal reduction technique.

6.2.3. Finite element method

In the following the details of the separated ENF, MSCB and $\mathrm{PENF_{II/III}}$ systems are discussed. The same models were used as those mentioned in Section 3. At the crack tip of the models singular elements were used and the mode-II and mode-III SERRs were evaluated by using the virtual crack-closure technique (VCCT) (Rybicki and Kanninen, 1977), the size of the crack tip elements were $\Delta x = \Delta y = 0.25$ mm and $\Delta z = 0.75$ mm (refer to Fig. 1 for the coordinate system).

End-notched flexure specimen. For the ENF test the boundary conditions for the finite element model were the same as those shown in Fig. 1a. The model was loaded at the center with a concentrated force of which value was determined from experimental crack initiation test. Then the mode-II SERR was determined by the VCCT method.

Modified split-cantilever beam. For the MSCB specimen the boundary conditions of the finite element model are demonstrated in Fig. 1b. The model was loaded at four points (see Fig. 1b). The load value was determined based on crack initiation tests. The mode-III SERR was calculated by the VCCT method.

Prestressed end-notched flexure specimen. The boundary conditions for the FE model of the $\mathrm{PENF_{II/III}}$ specimen are shown in Fig. 1c. On the one hand the model was loaded at the center by using the experimentally measured load values at crack initiation. This load provided the mode-II part of the mixed-mode II/III problem. On the other hand the model was also loaded at the plane of the delamination, as it is shown by Fig. 1c. The mode-III SERR component was controlled by using the prestressing rig, so this way the CTD was fixed. The values of the loads used in the FE analysis were calculated by using Eq. (29) at each six values of the CTD induced by prestressing ($\delta_{\mathrm{MSCB}} = 0.875$, 1.313, 1.750, 2.023, 2.188 and 2.297 mm), i.e., using the load-displacement relationship of the MSCB coupon. Finally, the VCCT method was used to obtain the mode-II and mode-III SERRs and the mode ratio.

The advantage of the FE technique is that the distribution of the SERRs along the crack front may be displayed and compared to experimental observations. Furthermore, it is possible to investigate cracks between bimaterial interfaces. On the contrary, the singularity at the crack tip, the large computational cost, as well as the increase of the mode-II SERR by refining the size of the crack tip elements should be mentioned as the relative drawbacks of the VCCT method.

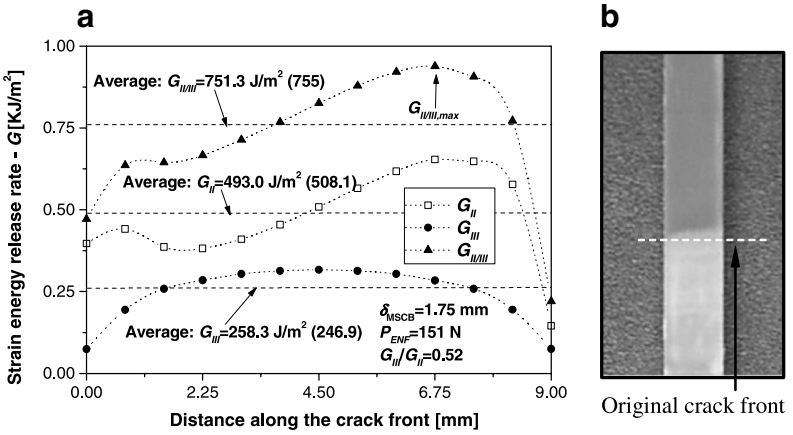

Fig. 10. The distribution of the mode-II and mode-III SERRs along the crack front in the $PENF_{II/III}$ specimen (a). The non-uniform crack front after crack initiation (b).

Fig. 10a shows the distribution of the SERR along the crack front in the case of $\delta_{MSCB} = 1.75$ mm and $P_{ENF} = 151$ N ($G_{III}/G_{II} = 0.52$). As it can be seen the mode-III SERR has a symmetric distribution along the crack front, while the mode-II and so the total SERRs are unsymmetric. The reason for that is both the ENF and MSCB loadings involve crack sliding displacements (CSD) near the crack front. While the CSD related to the ENF is rather uniform, then the CSD induced by the MSCB has approximately a linear distribution along the specimen width: the CSD by the MSCB loading is zero at the center of the crack front and reaches the maximum at the specimen sides, having opposite signs at the ends. If the $PENF_{II/III}$ specimen shows that the SERR distributions are unsymmetric then it may be assumed that in a real structure a quite similar condition exists. In other words the mixed-mode II/III condition involves inevitably the unsymmetric distribution also in the specimen and also in a real structure. If it is so then the SERR distribution in the $PENF_{II/III}$ specimen probably relates to practical conditions.

The work by Fernlund et al. (1995) applied the traditional SCB specimen and it has been mentioned that the SERRs (and the mode mix) vary along the crack front, therefore, the SCB specimen is not suitable for the determination of the fracture properties of composites. This is because at the specimen sides the mode-II component is dominant, while at the center a nearly pure mode-III condition exists. However, it is important to note that the SERR and the mode mix also changes along the crack front of the MMB specimen, despite there is a large number of works, which uses the MMB apparatus for the determination of fracture properties of composites (e.g., Reeder and Crews, 1990; Kim and Mayer, 2003). It should be highlighted that in the SCB specimen the change in the mode mix is more dramatic than in the MMB specimen. So, it seems that the variation of the mode mix along the crack front does not preclude the applicability of a system for the determination of the fracture properties of composite materials, although the degree of variation seems to be important.

To demonstrate the changes along the crack front the average values of the SERR distributions were calculated (see Fig. 10a) and were compared to the results of the improved beam model (see the values in the parentheses in Fig. 10a). The comparison shows a 4.4% difference for G_{III}, a -3% difference for G_{II} and a -0.5% difference for $G_{II/III}$. All of these results show the accuracy and the applicability of the analytical solution (Eqs. (4) and (12)) as a practical data reduction scheme.

Fig. 10b shows a propagated crack which has a curved shape. The reason for that is the non-uniformity of the total SERR along the crack front (Fig. 10a).

6.3. Critical strain energy release rates

Table 1 lists the mode mix, the mode-II, mode-III and the mixed-mode II/III SERRs at crack initiation as obtained by three data reduction schemes. The geometries tested had properties of $a = 55$ mm, $2h = 6.2$ mm,

Table 1
Critical energy release rates calculated by three reduction schemes

	δ_{MSCB} (mm)	0 (ENF)	0.875	1.313	1.750	2.023	2.188	2.297	2.48 (MSCB)
Improved beam theory (IBT)	G_{III}/G_{II}	0	0.09	0.21	0.49	1.03	1.51	3.82	∞
		—	±5e−3	±9e−3	±0.02	±0.06	±0.11	±0.41	—
	G_{III} (J/m^2)	0	61.7	138.9	246.9	330.1	385.8	425.3	445.7
	G_{II} (J/m^2)	802.1	700.3	649.7	508.1	322.4	256.6	112.6	0
		±19.2	±39.9	±27.2	±24.3	±20.3	±19.6	±12.6	—
	$G_{II/III}$ (J/m^2)	802.1	762.0	788.6	755.0	652.5	642.4	537.9	445.7
Compliance calibration (CC)	G_{III}/G_{II}	0	0.09	0.21	0.48	1.01	1.49	3.76	∞
		—	±5e−4	±9e−3	±2.3e−2	±0.06	±0.12	±0.41	—
	G_{III} (J/m^2)	0	62.3	140.2	249.3	333.3	389.5	429.5	460.8
	G_{II} (J/m^2)	824.0	719.5	667.5	522.1	331.2	263.6	115.7	0
		±23.5	±32.3	±20.9	±24.9	±18.4	±13.8	±10.1	—
	$G_{I/III}$(J/m^2)	824.0	781.8	807.7	771.4	664.5	653.1	545.2	460.8
Finite element method (FEM)	G_{III}/G_{II}	0	0.10	0.23	0.52	1.10	1.58	3.79	∞
	G_{III} (J/m^2)	0	65.1	145.7	258.3	345.8	403.0	446.1	477.8
	G_{II} (J/m^2)	770.9	670.3	628.5	493.0	316.9	254.9	117.5	0
	$G_{I/III}$ (J/m^2)	770.9	735.4	774.2	751.3	662.7	657.9	563.6	477.8

$s = 26$ mm and $2L = 150$ mm and at each value of the prestressing displacement (δ_{MSCB}) four coupons were used. The scatter is also given in the case of the mode ratio and the mode-II component. Since the mode-III SERR is fixed; the scatter of $G_{II/III}$ is equal to that of the G_{II}. From Table 1 it is obvious that the complete range of mode-mixity can be covered using the $PENF_{II/III}$ configuration.

The first block of Table 1 presents the results obtained by the IBT method, while the second shows the results of the CC method. The agreement between them is quite good, however in spite of that it should be mentioned that there is an inherent smoothing process (each specimen has the same dC/da) that comes into play by using a single CC curve for all specimens. Thus, some caution needs to be employed in generalizing the results and conclusions considering the CC method.

The last block of Table 1 presents the results obtained by using the finite element models. This time the scatter is not listed in Table 1 due to the large computational time, so the results were obtained by using the average values of the measured critical load values (P_{ENF}) by four specimens. Even the mode-II and the mode-III SERR components show the best correlation with the result of the IBT (first block in Table 1).

As a summary, for unidirectional composites the IBT is reliable and simple to apply, as it has been highlighted by other authors (e.g., Ducept et al., 1997; Ozdil and Carlsson, 1999a), while the CC method is unreliable due to certain reasons discussed in Section 6.2.2. On the other hand the application of the FEM as a data reduction method requires large computational time. So it is straightforward that at the present stage the optimal solution is the application of IBT for the evaluation of both the mode-II and mode-III SERRs.

The only problem is that it is possible that the additional material properties (E_{22}, E_{33}, G_{12}, G_{13}, ν_{12}, ν_{13}) are determined inaccurately. However, in a recent work the mixed-mode I/II version of the PENF was presented and experiments were performed for the same E-glass/polyester material (Szekrényes, 2006a). The results of the IBT technique were compared to that of the CC method leading to a very good agreement between them. It is well-known that the CC method is reliable for the data reduction in common mode-I and mode-II tests. So, it may be assumed that the additional material properties were determined with a proper accuracy for the $PENF_{I/II}$, and they can be utilized also for the $PENF_{II/III}$ system.

Finally, the effect of friction should be discussed. This effect may take place in both the ENF and MSCB specimens. In mode-II coupons (ENF, 4ENF, ELS and ONF) the frictional effect was investigated by Wang et al. (2003) using finite element models. The final conclusion was that the effect of friction on the SERR is small. Within the scope of present work a series ENF test was performed previously and the delamination plane was lubricated with grease. No difference in the compliance of the lubricated ENF compared to the original ENF test (Fig. 9a) was observed. In the MSCB specimen the frictional effect is assumed to be smaller due to the fact that the loading plane coincides with the delamination plane. Previous works by Chai (1988, 1990)

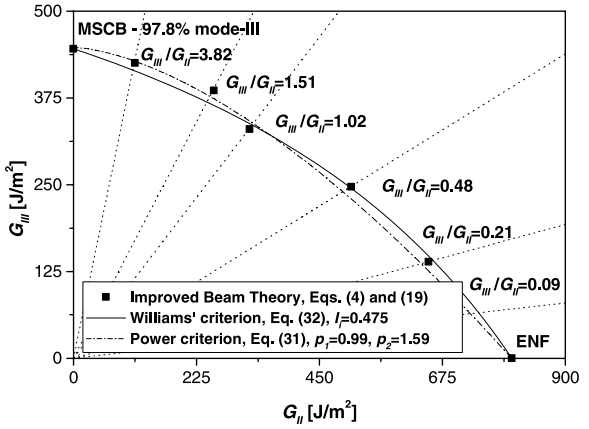

Fig. 11. Interlaminar fracture envelope for E-glass/polyester composite calculated by using IBT method.

on adhesively bonded joints showed that the mode-II and mode-III SERR components in DCB type tests were the same. Referring to Table 1 the pure mode-II toughness is significantly higher than the mode-III toughness. Based on the formers the reason for that is probably not the friction; however the elaboration of these problems requires further work.

6.4. Fracture envelopes

The different mixed-mode I/II fracture criteria were reviewed by Reeder (1992), Rikards et al. (1998) and Kim and Mayer (2003). It is assumed that these criteria are also applicable for a mixed-mode II/III case. We apply the two most popular criteria. In accordance with the traditional power criterion the following relation may be established between the mode-II and mode-III strain energy release rates (e.g., Hashemi et al., 1990b):

$$\left(\frac{G_{\mathrm{II}}}{G_{\mathrm{IIC}}}\right)^{p_1}+\left(\frac{G_{\mathrm{III}}}{G_{\mathrm{IIIC}}}\right)^{p_2}=1. \tag{31}$$

On the other hand Williams' criterion (e.g., Hashemi et al., 1990a,b) recommends the following expression:

$$\left(\frac{G_{\mathrm{II}}}{G_{\mathrm{IIC}}}-1\right)\left(\frac{G_{\mathrm{III}}}{G_{\mathrm{IIIC}}}-1\right)-I_i\left(\frac{G_{\mathrm{II}}}{G_{\mathrm{IIC}}}\right)\left(\frac{G_{\mathrm{III}}}{G_{\mathrm{IIIC}}}\right)=0, \tag{32}$$

where I_i is the interaction parameter between the mode-I and mode-II SERRs. If $I_i=0$ then there is no interaction. Also, if $I_i=1$ then Eq. (32) states a simple addition. In Eqs. (31) and (32) G_{IIC} is the critical SERR under pure mode-II (calculated from the data of the ENF specimen), G_{IIIC} is the mode-III critical SERR (calculated from the data of the MSCB specimen). The results of the $\mathrm{PENF_{II/III}}$ test (listed in Table 1) were used to provide six additional points in the G_{II}–G_{III} plane. The power parameters (p_1, p_2) in Eq. (31) and the interaction parameter (I_i) in Eq. (32) were determined by a curve-fit technique.

The fracture envelope calculated by using the IBT method is displayed in Fig. 11. The main conclusion is that there is a significant interaction between the mode-II and mode-III SERRs. Overall, the difference between the power and Williams' criteria is negligible, both describes the same failure locus. However, the application of Williams' method is simpler.

6.5. Comparison of the fracture envelopes in the G_I–G_{II} and G_{II}–G_{III} planes

In a recent work, the fracture envelope in the G_{I}–G_{II} plane was determined by the mixed-mode I/II version of the PENF specimen ($\mathrm{PENF_{I/II}}$) for the same E-glass/polyester material (Szekrényes, 2006a). A similar experimental study resulted in a concave envelope as it is shown in Fig. 12. Based on a comparison between

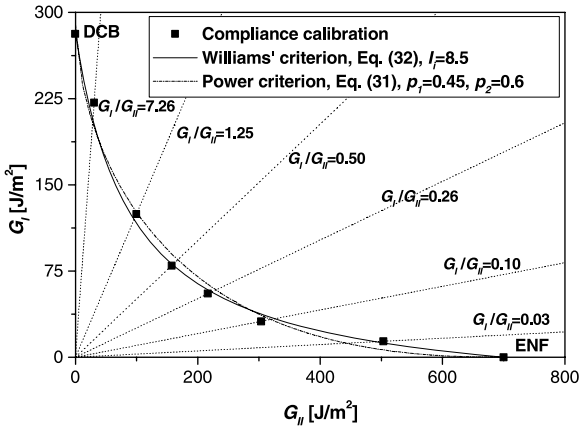

Fig. 12. Interlaminar fracture envelope in the G_I–G_{II} plane for E-glass/polyester composite calculated by CC method.

Figs. 11 and 12 we may conclude that the material behaves differently under mixed-mode I/II and mixed-mode II/III loading conditions, however, interaction takes place in both cases.

7. Conclusions

In this work, the mixed-mode II/III version of the prestressed end-notched flexure specimen was developed for interlaminar fracture testing of laminated transparent composite materials. Apart from the MSCB and the traditional ENF tests the $PENF_{II/III}$ specimen was used to obtain the mixed-mode II/III strain energy release rate at crack propagation onset including six different mode ratios. To perform the experiments unidirectional E-glass/polyester specimens were manufactured. The measured data was reduced using three different approximations: improved beam theory, compliance calibration and the finite element method. The compliance calibration method – which is known as an accurate technique for common mode-I and mode-II tests – was not recommended due to certain reasons. Furthermore, the numerical model validated the analytical solution, therefore, the improved beam model was recommended for the evaluation of both the mode-I and mode-II strain energy release rates.

The fracture envelope of the present material was determined using two criteria: the power criterion and another one by Williams. In each case both predicted the same failure locus. The obtained results were compared to a fracture envelope in the G_I–G_{II} plane determined for the same material. The difference between the nature of the fracture envelopes was attributed to the fact that the material behaves differently in the G_I–G_{II} than in the G_{II}–G_{III} plane.

The $PENF_{II/III}$ specimen offers several advantages. First, it requires the traditional beam-like specimen geometry. Second, it was shown that the $PENF_{II/III}$ specimen is able to produce any mode ratio at crack propagation onset. During the test no large displacements and geometrical nonlinearities were observed. The drawbacks of the PENF specimen are that the mode ratio changes with the crack length and the applied load, so the method is recommended mainly for the testing of transparent composite materials. Finally, the mode ratio can not be calculated without performing experiments (i.e., it can not be designed before the test), involving the fact that the mode ratio will depend on the definition of the crack initiation and the accuracy of the measurement of the load and crack length.

Acknowledgments

This research work was sponsored by the Hungarian Ministry of Education (OM) under Grant No. T30833-066 (41). The author is grateful to Alfredo Balacó de Morais for the reference by Davies et al. (1996). I wish to thank Barry D. Davidson for sending his work (Davidson and Sundararaman, 1996) to me.

References

Anderson, T.L., 2005. Fracture Mechanics – Fundamentals and Applications, third ed. CRC Press, Taylor & Francis Group, Boca Raton, London, New York, Singapore.

Bao, G., Ho, S., Suo, Z., Fan, B., 1992. The role of material orthotropy in fracture specimens for composites. International Journal of Solids and Structures 29, 1105–1116.

Becht, G., Gillespie Jr., J.W., 1988. Design and analysis of the crack rail shear specimen for mode III interlaminar fracture. Composites Science and Technology 31, 143–157.

Bradley, W.L., Cohen, R.N. 1985. Matrix deformation and fracture in graphite-reinforced epoxies. In: Johnson, S.W. (Ed.), Delamination and Debonding of Materials, American Society for Testing and Materials, Philadelphia, ASTM STP 876, pp. 389–410.

Carlsson, L.A., Gillespie, J.W., Pipes, R.B., 1986. On the analysis and design of the end notched flexure (ENF) specimen for mode II testing. Journal of Composite Materials 20, 594–604.

Chai, H., 1988. Shear fracture. International Journal of Fracture 37, 137–159.

Chai, H., 1990. Interlaminar shear fracture of laminated composites. International Journal of Fracture 43, 117–131.

Chen, L., Sankar, B.V., Ifju, P.G. 2003. Mixed-Mode Fracture Toughness Tests for Stitched Composite Laminates. AIAA Paper 2003-1874. In: Proceedings of the 44th AIAA Structures, Structural Dynamics and Materials Conference, Norfolk, Virginia, April 7–10, 2003, 10 pages.

Cicci, D., Sharif, F., Kortschot, M.T. 1995. Data reduction for the split cantilever beam mode III delamination test. In: Proceedings, ACCM 10, Whistler, British Columbia, Canada, August 14–18.

Crews Jr., J.H., Reeder, J.R., 1988. A mixed-mode bending apparatus for delamination testing. NASA Technical Memorandum 100662, 1–37.

Davidson, B.D., Krüger, R., König, M., 1995. Three-dimensional analysis of center-delaminated unidirectional and multidirectional single-leg bending specimens. Composites Science and Technology 54, 385–394.

Davidson, B.D., Sundararaman, V., 1996. A single leg bending test for interfacial fracture toughness determination. International Journal of Fracture 78, 193–210.

Davies, P., Ducept, F., Brunner, A.J., Blackman, B.R.K., Morais, de A.B. 1996. Development of a standard mode II shear fracture test procedure. In: Proceedings of the 7th European Conference on Composite Materials (ECCM-7), vol. 2, London, May, pp. 9–15.

Donaldson, S.L., 1988. Mode III intelaminar fracture characterization of composite materials. Composites Science and Technology 32, 225–249.

Ducept, F., Davies, P., Gamby, D., 1997. An experimental study to validate tests used to determine mixed mode failure criteria of glass/epoxy composites. Composites Part A: Applied Science and Manufacturing 28A, 719–729.

Edde, F.C., Verreman, Y., 1995. Nominally constant strain energy release rate specimen for the study of mode II fracture and fatigue in adhesively bonded joints. International Journal of Adhesion and Adhesives 15, 29–32.

Ehart, R.J.A., Stanzl-Tschegg, S.E., Tschegg, E.K., 1998. Crack face interaction and mixed.mode fracture of wood composites during mode III loading. Engineering Fracture Mechanics 61, 253–278.

Ehart, R.J.A., Stanzl-Tschegg, S.E., Tschegg, E.K., 1999. Mode III fracture energy of wood composites in comparison to solid wood. Wood Science Technology 33, 391–405.

Farshad, M., Flüeler, P., 1998. Investigation of mode III fracture toughness using an anti-clastic plate bending method. Engineering Fracture Mechanics 60, 5–6.

Fernlund, G., Lanting, H., Spelt, J.K., 1995. Mixed mode II–mode III fracture of adhesive joints. Journal of Composite Technology and Research 17 (4), 14.

Hashemi, S., Kinloch, J., Williams, J.G., 1987. Interlaminar fracture of composite materialsProceedings of the 6th ICCM and ECCM Conference, vol. 3. Elsevier Applied Science, London, pp. 3.254–3.264.

Hashemi, S., Kinloch, J., Williams, J.G., 1990a. The effects of geometry, rate and temperature on mode I, mode II and mixed-mode I/II interlaminar fracture toughness of carbon-fibre/poly(ether–ether ketone) composites. Journal of Composite Materials 24, 918–956.

Hashemi, S., Kinloch, J., Williams, J.G., 1990b. Mechanics and mechanisms of delamination in a poly(ether sulphone)-fibre composite. Composites Science and Technology 37, 429–462.

Hwang, S.-F., Hu, C.-L., 2001. Tearing mode interlaminar fracture toughness of composite materials. Polymer Composites 22, 57–64.

Ifju, P.G., Chen, L.-S., Sankar, B.V. 2002. Mixed-mode fracture toughness for stitched composites. SEM Annual Conference, Milwaukee, WI 2002, paper number 173.

Kamat, S.V., Srinivas, M., Rao, P.R., 1998. Mixed mode I/III fracture toughness of armco iron. Acta Materialia 46 (14), 4985–4992.

Kim, B.W., Mayer, A.H., 2003. Influence of fiber direction and mixed-mode ratio on delamination fracture toughness of carbon/epoxy laminates. Composites Science and Technology 63, 695–713.

Lazarus, V., Leblond, J.-B., Mouschrif, S.-E., 2001. Crack fornt rotation and segmentation in mixed mode I+III or I+II+III. Part II: Comparison with experiments. Journal of the Mechanics and Physics of Solids 49, 1421–1443.

Lee, S.M., 1993. An edge crack torsion method for mode III delamination fracture testing. Journal of Composites Technology and Research 15 (3), 193–201.

Li, H., Jones, R.H., Hirth, J.P., 1995. Mixed mode I/III fracture toughness of a V-5Cr-5Ti alloy at 100 °C. Scripta Metallurgica et Materialia 32 (4), 611–616.

Liao, W.C., Sun, C.T., 1996. The determination of mode III fracture toughness in thick composite laminates. Composites Science and Technology 56, 489–499.

Naik, N.K., Reddy, K.S., Meduri, S., Raju, N.B., Prasad, P.D., Azad, S.K.N.M., Ogde, P.A., Reddy, B.C.K., 2002. Interlaminar fracture characterization for plain weave fabric composites. Journal of Materials Science 37, 2983–2987.

Olsson, R., 1992. A simplified improved beam analysis of the DCB specimen. Composites Science and Technology 43, 329–338.

Ozdil, F., Carlsson, L.A., 1999a. Beam analysis of angle-ply laminate DCB specimens. Composites Science and Technology 59, 305–315.

Podczeck, F., 2001. The determination of fracture mechanics properties of pharmaceutical materials in mode III loading using an anti-clastic plate bending method. International Journal of Pharmaceutics 227, 39–46.

Qiao, P., Wang, J., Davalos, J.F., 2003b. Analysis of tapered ENF specimen and characterization of bonded interface fracture under mode-II loading. International Journal of Solids and Structures 40, 1865–1884.

Reeder, J.R., 1992. An evaluation of mixed-mode delamination failure criterion. NASA Technical Memorandum 104210, 1–49.

Reeder, J.R., Crews Jr., J.H., 1990. Mixed-mode bending method for delamination testing. AIAA Journal 28, 1270–1276.

Rikards, R., Buchholz, F.G., Wang, H., Bledzki, A.K., Korjakin, A., Richard, H.-A., 1998. Investigation of mixed mode I/II interlaminar fracture toughness of laminated composites by using a CTS type specimen. Engineering Fracture Mechanics 61, 325–342.

Rybicki, E.F., Kanninen, M.F., 1977. A finite element calculation of stress intensity factors by a modified crack closure integral. Engineering Fracture Mechanics 9, 931–938.

Schön, J., Nyman, T., Blom, A., Ansell, H., 2000. Numerical and experimental investigation of a composite ENF-specimen. Engineering Fracture Mechanics 65, 405–433.

Schuecker, C., Davidson, B.D., 2000. Evaluation of the accuracy of the four-point bend end-notched flexure test for mode II delamination toughness determination. Composites Science and Technology 60, 2137–2146.

Sharif, F., Kortschot, M.T., Martin, R.H. 1995. Mode III delamination using a split cantilever beam. In: Martin, R.H. (Ed.), Composite Materials: Fatigue and Fracture, vol. 5, ASTM STP 1230, ASTM, Philadelphia, pp. 85–99.

Sørensen, B.F., Jørgensen, K., Jacobsen, T.K., Østergaard, R.C. 2004. A general mixed-mode fracture specimen: the DCB specimen loaded with uneven bending moments. Print. Pitney Bowes Management Services A/S - Risø-R-1394(EN), 1–35.

Suemasu, H., 1999. An experimental method to measure the mode-III interlaminar fracture toughness of composite materials''. Composites Science and Technology 59, 1015–1021.

Szekrényes, A. 2005. Delamination of composite specimens. Ph.D. Thesis, Budapest University of Technology and Economics, Faculty of Mechanical Engineering, Department of Applied Mechanics, Budapest, PhD-261/2004.

Szekrényes, A., 2006a. Prestressed fracture specimen for delamination testing of composites. International Journal of Fracture 139, 213–237.

Szekrényes, A., submitted for publication, 2006b. Improved analysis of the modified split-cantilever beam for mode-III fracture. Cement and Concrete Composites.

Szekrényes, A., Uj, J., 2005. Mode-II fracture in E-glass/polyester composite. Journal of Composite Materials 39 (19), 1747–1768.

Szekrényes, A., Uj, J., 2006. Comparison of some improved solutions for mixed-mode composite delamination coupons. Composite Structures 72, 321–329.

Trakas, K., Kortschot, M.T. 1997. The relationship between critical strain energy release rate and fracture mode multidirectional carbon-fiber/epoxy laminates. In: Armanios, E.A. (Ed.), Composite Materials: Fatigue and Fracture, vol. 6, ASTM STP 1285, ASTM, pp. 283–304.

Wang, H., Vu-Khanh, T., 1996. Use of end-loaded-split (ELS) test to study stable fracture behaviour of composites under mode-II loading. Composite Structures 36, 71–79.

Wang, J., Qiao, P., 2004. Novel beam analysis of the end notched flexure specimen for mode-II fracture. Engineering Fracture Mechanics 71, 219–231.

Wang, W.-X., Takao, Y., Nakata, M. 2003. Effects of friction on the measurement of the mode II interlaminar fracture toughness of composite laminates. In: Proceedings of the 14th International Conference on Composite Materials (CD-ROM), Manuscript No.: 1429, July 14–18, San Diego, California, USA.

Williams, J.G., 1989. End corrections for orthotropic DCB specimens. Composites Science and Technology 35, 367–376.

Yoshihara, H., 2006. Examination of the 4-ENF test for measuring the mode III R-curve of wood. Engineering Fracture Mechanics 73, 42–63.